On Refining the Input Data Set
to
Mathematical Models Simulating Arterial blood flow in Humans

KARTHIK ALASAKANI, RADHIKA S.L. TANTRAVAHI, PRAVEEN KUMAR PTV
Department of Mathematics,
Birla Institute of Technology and Science, Pilani, Hyderabad Campus
Hyderabad, Telangana, 500078
INDIA

Abstract: - In this paper, we worked on methods to reduce the input data set to the mathematical models developed to simulate blood flow through human arteries. In general, any mathematical model designed to mimic a natural process needs specific information on its model parameters. In our models, the inputs to these parameters are from the human arterial system, i.e., the anatomical data on arteries and physiological information on blood. Besides, few other parameters in the models describe mechanisms, such as the arteries' elastic behaviour. These mechanisms described using mathematical relations help assign values to the parameters satisfying specific mathematical requirements. In general, the clinical data or the mathematical requirements provide a range of permissible values for the model parameters. However, we assign only a finite number of values in the range to the parameters to carry out simulations. Even though the values assigned to the parameters significantly differ from each other in magnitude, there is a possibility that some of these data sets mimic the same state of the system (arterial system). And identifying such data sets is not an apparent task but requires robust procedures. Thus, in this work, we attempt to shed light on a data size reduction technique to identify all such values and remove them from the input data set. We propose the statistical testing procedures to identify a significant difference in the dependent variables' values (computed using the developed mathematical models) with the independent variables (the model parameters).

Key-Words: - Mathematical model, elastic pipe, arterial blood flow, simulation, non-parametric test, statistical analysis.

Abbreviations

$\vec{q}$	– Velocity vector	η_1, η_1'	– Couple stress momentum coefficients
p	– Thermodynamic pressure	C	– Dimensionless couple stress parameter
ρ	– Density (kg/m^3)	$\vec{c}$	– Body moment per unit mass
τ_{ij}	– Deviatoric stress tensor	σ	– Couple stress parameter
δ_{ij}	– Kronecker symbol	a_0	– Average blood pressure ($Pa.\,m^{-1}$)
μ	– Viscosity ($Pa.\,s$)	a_1	– Pulse difference ($Pa.\,m^{-1}$)
e_{ij}	– Rate of deformation tensor	Ω	– Frequency of oscillations ($2\pi \cdot HR$)
t_{ij}	– Non-symmetric stress tensor	HR	– Heart rate
m_{ij}	– Couple Stress tensor	f	– Taper fraction
$t_{ij}^{(s)}$	– Symmetric part of t_{ij}	L	– Length of the artery
$t_{ij}^{(A)}$	– Skew-symmetric part of t_{ij}	R_0	– Inlet radius (at $t = 0$)
d_{ij}	– Rate of deformation tensor	β	– Contracting/Expanding parameter
c_k	– k-component of body moment vector	Δ	– Aspect ratio $\left(\frac{R_0}{L}\right)$
ε_{ijk}	– Levi-Civita symbol	α	– Womersley number $\left(\sqrt{\frac{\rho\Omega R_0^2}{\mu}}\right)$
m	– Trace of m_{ij}		
λ	– Couple stress viscosity coefficient	WSS	– Wall shear stress ($N.\,m^{-2}$)
H_1^{N}	– 1st Homotopy function in Newtonian Model	QF	– Volumetric flow rate ($m^3.s^{-1}$)
		H_1^{C}	– 1st Homotopy function in Couple Stress Model

H_2^N – 2nd Homotopy function in Newtonian Model

H_2^C – 2nd Homotopy function in Couple Stress Model

1 Introduction

Scientific modelling of a natural or biological phenomenon helps understand a complicated process's underlying mechanism and identify the factors that affect it. These models can be physical, conceptual, or mathematical. One chooses a convenient mode based on the problem chosen for study and their objectives. As seen in the literature concerning the research on the arterial blood flow in humans, most researchers adopted mathematical modelling for the problem. One possible reason could be that the blood flow in human arteries involves several complicated mechanisms that need precise models for drawing reliable conclusions. Another motive could be the ease with which simulations can be carried with the developed mathematical models to mimic the arterial system's various states, as seen in the following works.

Tu et al. described how computational hemodynamics could be applied to the cardiovascular system study [1]. Quarteroni (2001) has touched upon several challenges in modelling the human cardiovascular system mathematically [2]. Sankar and Lee studied the blood flow through the artery with mild stenosis, considering the flow to be pulsatile and the blood as Heschel–Bulkley fluid [3]. Blanco et al. developed a 1D-3D coupled model to study the complex interactions in the arterial network and specific arterial segments. They provided some applications of their model that are of potential clinical interest [4]. Formaggia et al. modelled pulse (blood) propagation in compliant arteries using a family of 1D non-linear systems [5]. Ho et al. performed CFD analysis on cerebral aneurysms by using the coupled 1D-3D approach. They constructed the arterial tree's geometric model in 1D and the aneurysm in 3D from a 3D Computed Tomography Angiography image [6]. Kroon et al. simulated the vascular hemodynamics using a coupled 0D-1D model. The large arteries are modelled using a 1D wave propagation model, and the small arteries in the periphery using a 0D lumped model [7]. Liang et al. developed a multiscale model of the cardiovascular system by coupling a 1D model with a 0D lumped parameter model to study the effects of aortic valvular and arterial stenoses on global hemodynamics. Their model predicted a significant effect of the location of stenoses on global hemodynamics [8]. Malossi et al. devised a numerical scheme for solving implicitly coupled 1D/3D model developed for blood flow in compliant vessels [9]. Olufsen et al. considered the axisymmetric flow of blood in large systemic arteries modelled as tapered and compliant vessels. Their simulations agreed well with a person's magnetic resonance measurements in nine peripheral locations and the ascending aorta [10]. Bartosik studied turbulent blood flow in the aorta and examined the effects of frictional losses on yield shear stress [11].

The present work also adopts mathematical modelling. We aim to tune the blood flow models developed for large and small arteries to mimic the arterial system for different age groups among male and female populations. This work on fine-tuning the developed mathematical models to suit different age groups and genders is possibly the first of its kind and thus taken for study.

Firstly, we develop mathematical models for the small and large arteries in the human arterial system and simulate them to mimic the different arterial states. The mathematical models are developed, incorporating the system's salient features. We used the published data on the human arterial system's anatomy and physiology for different age groups and genders to carry out simulations. Besides these, we also input a few data based on the mathematical specifications of the developed models. In most cases, we see that the data assume values over a specified range, and one needs to choose a finite number of values from that range to carry out simulations. In doing so, our perception is that some of the data sets mimic the same arterial state, and identifying such data sets (if any) forms our next objective.

The mathematical model built to mimic the blood flow in the human arterial system has to include specific means, through mathematical expressions to describe the system's salient features, such as (i) the pulsatile pressure gradient induced by the heart to enable the blood flow (ii) blood, a complex fluid that is a suspension of particles and (iii) the arteries, elastic pipes with tapering and branching. These mathematical expressions comprise parameters to describe the arterial system's features. Based on their function, we classified these parameters into three

sets: flow, fluid, and mechanical, and they assume inputs to mimic the arterial system's different states.

As mentioned earlier, in general, the inputs to model parameters are either from clinical data or due to mathematical constraints imposed by the mathematical models used. For instance, parameters, such as heart rate, blood pressure, blood viscosity, etc., assume values over a range based on the anatomical and physiological data related to the blood flow in human arteries. And parameters used to describe mechanisms or processes like an artery's response under various stress conditions are assigned values from a specified range based on the mathematical requirements/ constraints. To identify the data sets that mimic the same arterial state, we work on statistical tests and refine the input data set. To perform statistical analysis, we test the input data set for its significance on two physical quantities: wall shear stress (WSS) and volumetric flow rate (QF) computed from the mathematical models built.

The paper is organised as follows: Section 2 details the mathematical description of the human arterial system's various features: the blood, the artery, and the blood flow. To incorporate the human arterial system's salient features: Blood is taken as a Newtonian [12] or a non-Newtonian fluid described via the models in the works [13-15]. In this paper, we chose to develop two models, one with blood as the Newtonian fluid and the other as the couple stress fluid. The artery is modelled as a tapered circular pipe with elastic nature described by an expanding/contracting parameter [16, 17]. The blood flow is assumed to be under the influence of a pulsatile pressure gradient described by Mandal [18]. Mathematical models are developed using the flow governing equations in transport phenomena with appropriate boundary conditions. In Section 3, we brief the Homotopy Analysis Method (HAM) to solve the models developed [19, 20]. Section 4 presents the data (as Tables) on healthy humans to carry out simulations. These tables show the anatomical data on human arteries and physiological data on blood flow for male and female populations of different age groups ranging from 19 to 60 [21-25]. We also see the fluid and mechanical parameters' values satisfying the required mathematical constraints as detailed in references [13, 16, 21]. In Section 5, the statistical testing process wherein the objectives, the test statistic, and result analysis are detailed. We present the conclusions and remarks in Section 6.

2 Mathematical Model

As mentioned earlier, blood flow through the human artery is modelled as the fluid flow in a circular, and tapered elastic pipe wherein an oscillatory pressure gradient drives the flow. Cylindrical polar coordinate system (r, θ, z) (where r and z are the radial and axial coordinates, respectively, and θ is the azimuthal angle) is used to describe the problem's geometry, and the fluid (blood) flow is assumed to be in the z-direction. Further, the fluid is considered incompressible and the flow axisymmetric so that the components of the velocity $(\vec{q})$, and the thermodynamic pressure, denoted by p, are functions only of r, z and time t. Thus, the velocity vector is $\vec{q}(r, z, t) = \big(u(r, z, t), 0, w(r, z, t)\big)$, and the thermodynamic pressure p is $p(r, z, t)$.

2.1 Mathematical formulation of the problem

Fluid (blood) flow is governed by the Navier-Stokes equations that take the form: [12]

$$\frac{\partial u}{\partial r} + \frac{u}{r} + \frac{\partial w}{\partial z} = 0 \tag{1}$$

$$\frac{\partial u}{\partial t} + u\frac{\partial u}{\partial r} + w\frac{\partial u}{\partial z} = -\frac{1}{\rho}\frac{\partial p}{\partial r} - \frac{1}{\rho}\left(\frac{1}{r}\frac{\partial}{\partial r}(r\tau_{rr}) + \frac{\partial}{\partial z}(\tau_{rz})\right) \tag{2}$$

$$\frac{\partial w}{\partial t} + u\frac{\partial w}{\partial r} + w\frac{\partial w}{\partial z} = -\frac{1}{\rho}\frac{\partial p}{\partial z} - \frac{1}{\rho}\left(\frac{1}{r}\frac{\partial}{\partial r}(r\tau_{rz}) + \frac{\partial}{\partial z}(\tau_{zz})\right) \tag{3}$$

We assumed that the radial flow velocity and the convective acceleration terms are of a smaller order of magnitude with respect to the axial flow velocity and the local acceleration terms, respectively [12]. Hence the radial momentum equation (2) reduces to:

$$-\frac{\partial p}{\partial r} = 0 \tag{4}$$

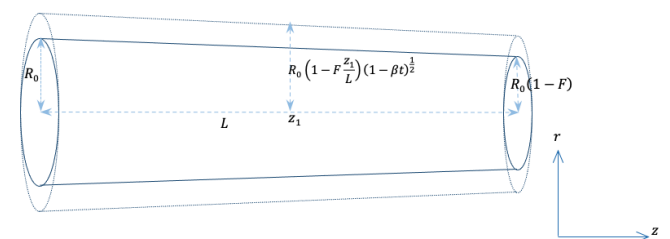Equation (4) indicates that the pressure function is independent of r.

Fig. 1: Schematic diagram showing the expansion phase

2.2 Model for the human artery

Since arteries are tapered and elastic pipes, we modified the models proposed by Uchida and Aoki

[16] and Karthik et al. [17] as follows to incorporate the elastic behaviour as described in [16] and the taper in [17] as follows:

$$R(z,t) = R_0 \left(1 - f\frac{z}{L}\right)(1 - \beta\Omega t)^{\frac{1}{2}} \quad (5)$$

Here β is a contraction/expansion coefficient that takes any real value. Positive values of β indicate the contraction state of the pipe, while negative values of this parameter describe the expansion state. R_0 denotes the pipe's radius at the inlet when the time $t = 0$. f is the fraction of tapering that takes any value between 0 and 1. L is the pipe's length and $\Omega = 2\pi \cdot HR/60$, HR being the number of heartbeats per minute [16, 17].

2.3 Model for the blood

As mentioned earlier, we considered two mathematical models, namely, Newtonian and Couple Stress fluid, to describe the fluid, i.e., the blood [12, 13]. The Newtonian model describes blood as having a linear stress-strain relationship, most accurate for its large arteries flow. The Couple Stress fluid model is a non-Newtonian model best suited to describe the artery's non-linear stress-strain relationship.

2.3.1 Newtonian fluid model

Constitutive equation for Newtonian fluid is given by [12]

$$\tau_{ij} = -p\delta_{ij} + 2\mu e_{ij} \quad (6)$$

Using the constitutive equation (6), equations (1) and (3) take the form:

$$\frac{\partial u}{\partial r} + \frac{1}{r}u + \frac{\partial w}{\partial z} = 0 \quad (7)$$

$$\rho\left(\frac{\partial w}{\partial t} + u\frac{\partial w}{\partial r} + w\frac{\partial w}{\partial z}\right) = -\frac{\partial p}{\partial z} + \mu\left(\frac{1}{r}\frac{\partial}{\partial r}\left(r\frac{\partial w}{\partial r}\right) + \frac{\partial^2 w}{\partial z^2}\right). \quad (8)$$

By introducing the dimensionless variables,

$$w^* = \frac{w}{\omega L}, \; t^* = t\omega, \; u^* = \frac{u}{\omega R_0}, \; z^* = \frac{z}{L} \; \text{and} \; r^* = \frac{r}{R_0} \quad (9)$$

equations (7) and (8) take the form (after dropping *),

$$\frac{\partial u}{\partial r} + \frac{1}{r}u + \frac{\partial w}{\partial z} = 0 \quad (10)$$

$$\frac{\partial w}{\partial t} + u\frac{\partial w}{\partial r} + w\frac{\partial w}{\partial z} = -P^* - \frac{1}{\alpha^2}\left(\frac{\partial^2 w}{\partial r^2} + \frac{1}{r}\frac{\partial w}{\partial r} + \Delta^2\frac{\partial^2 w}{\partial z^2}\right) \quad (11)$$

where $P^* = -\frac{1}{\rho\Omega^2 L^2}\frac{\partial P}{\partial z}$ is the non-dimensional pressure gradient, $\Delta = \frac{R_0}{L}$ is termed as the aspect ratio and $\alpha = \sqrt{\frac{\rho\Omega R_0^2}{\mu}}$ is the Womersley number.

The boundary conditions in the non-dimensional form are:

$$u = \frac{\partial R}{\partial t}(z,t), w = 0 \text{ on } r = R(z,t)$$
$$u = 0, \frac{\partial w}{\partial r} = 0 \text{ at } r = 0 \quad (12)$$

where, $R(z,t) = (1 - fz)(1 - \beta t)^{0.5}$ (the non-dimensional form of expression (5) $\quad (13)$

2.3.2 Couple stress fluid model

The couple stress fluid model assumes that the fluid medium can sustain couple stresses [13]. Thus the non-symmetric stress tensor t_{ij} and the couple stress tensor m_{ij} are given by: $t_{ij} = t_{ij}^{(s)} + t_{ij}^{(A)}$,

where, $t_{ij}^{(s)} = -p\delta_{ij} + \lambda div(\vec{q})\delta_{ij} + 2\mu d_{ij}$, and

$$t_{ij}^{(A)} = -\frac{1}{2}\varepsilon_{ijk}\left(m_{,k} - 4\eta_1\omega_{i,jkk} + \rho c_k\right). \quad (14)$$

$$m_{ij} = \frac{1}{3}m\delta_{ij} + 4\eta_1\omega_{j,i} + 4\eta_1'\omega_{i,j}. \quad (15)$$

Here $t_{ij}^{(s)}$ is the symmetric part of the stress tensor, $t_{ij}^{(A)}$ is the skew-symmetric part of the stress tensor, $\omega_{i,j} = \frac{\partial\omega_i}{\partial x_j}$ is the derivative of the ith component of $\vec{\omega} = \frac{1}{2}curl\,\vec{q}$, d_{ij} is the rate of deformation tensor, c_k is the k-component of body moment vector, δ_{ij} denotes Kronecker symbol, ε_{ijk} is the Levi-Civita symbol, m is the trace of the couple stress tensor m_{ij}, and $m_{,k} = grad(m)$, $\omega_{i,jkk}$ represents $grad(\nabla^2\omega_i)$.

The quantities λ and μ are the couple stress viscosity coefficients, while η_1 and η_1' are the couple stress momentum coefficients. These coefficients are material constants and are constrained by the inequalities:

$$\mu \geq 0, 3\lambda + 2\mu \geq 0, \eta_1 \geq 0, |\eta_1'| \leq \eta_1. \quad (16)$$

Under the assumptions on the flow mentioned earlier and using the constitutive equations given in (14)-(15), the continuity equation and the momentum equation shown in (1) and (3) reduce to

$$\frac{\partial u}{\partial r} + \frac{1}{r}u + \frac{\partial w}{\partial z} = 0 \quad (17)$$

$$\rho\left(\frac{\partial w}{\partial t} + u\frac{\partial w}{\partial r} + w\frac{\partial w}{\partial z}\right) = -\frac{\partial p}{\partial z} - \mu\left(\frac{\partial^2 w}{\partial r^2} + \frac{1}{r}\frac{\partial w}{\partial r}\right) -$$
$$\eta_1\left(\frac{\partial^4 w}{\partial r^4} - \frac{2}{r}\frac{\partial^3 w}{\partial r^3} - \frac{1}{r^2}\frac{\partial^2 w}{\partial r^2} + \frac{1}{r^3}\frac{\partial w}{\partial r} + \frac{1}{r}\frac{\partial^3 w}{\partial r\partial z^2} + \frac{\partial^4 w}{\partial r^2\partial z^2} + \frac{\partial^4 w}{\partial z^4}\right) \quad (18)$$

By using the dimensionless variables introduced in (9), equation (18) (after dropping *) takes the form:

$$\frac{\partial w}{\partial t} + u\frac{\partial w}{\partial r} + w\frac{\partial w}{\partial z} = -P^* - \frac{1}{\alpha^2}\left(\frac{\partial^2 w}{\partial r^2} + \frac{1}{r}\frac{\partial w}{\partial r}\right) -$$
$$C\left(\frac{\partial^4 w}{\partial r^4} - \frac{2}{r}\frac{\partial^3 w}{\partial r^3} - \frac{1}{r^2}\frac{\partial^2 w}{\partial r^2} + \frac{1}{r^3}\frac{\partial w}{\partial r} + \Delta^2\left(\frac{1}{r}\frac{\partial^3 w}{\partial r\partial z^2} + \frac{\partial^4 w}{\partial r^2\partial z^2} + \Delta^2\frac{\partial^4 w}{\partial z^4}\right)\right) \quad (19)$$

where $\Delta = \frac{R_0}{L}$ termed as the aspect ratio, $P^* = \frac{1}{\rho\Omega^2 L^2}\frac{\partial p}{\partial z}$ is the dimensionless pressure, $\alpha = \sqrt{\frac{\rho\Omega R_0^2}{\mu}}$ is the Womersley number, and $C = \frac{\eta_1}{\rho\Omega R_0^4}$ is the couple stress parameter.

The mathematical representation of the boundary conditions in the non-dimensional form is,

(i) $u = \frac{dR}{dt}, w = 0$ on $r = R(z,t)$
   (no-slip boundary condition),

(ii) $\frac{\partial^2 w}{\partial r^2} - \frac{\sigma}{r}\frac{\partial w}{\partial r} = 0$ on $r = R(z,t)$ with $\sigma = \frac{\eta_1}{\eta_1'}$,
   (couple stresses vanish on the wall),

(iii) $\frac{\partial^2 w}{\partial r^2} - \frac{\sigma}{r}\frac{\partial w}{\partial r}$ is finite at $r = 0$,

(iv) $\frac{\partial w}{\partial r} = 0$ at $r = 0$
   (velocity is finite at the center of the tube).
   $\qquad\qquad\qquad\qquad\qquad\qquad (20)$

2.4 Model for the blood flow
Because of the oscillatory nature of the blood flow, the pressure gradient takes the form:

$$-\frac{\partial p}{\partial z} = a_0 + a_1\cos\Omega t, t \geq 0 \quad (21)$$

where a_0 is the average blood pressure, a_1 is the constant amplitude of the pressure gradient ($Pa. m^{-1}$) and $\Omega = 2\pi \cdot HR/60$, HR being the number of heartbeats per minute [18].

3 Method of Solution
We used the HAM (Homotopy Analysis method) to find the solution to the developed mathematical models. This method introduced by Liao is an extension of the He's Homotopy perturbation method (HPM), a semi-analytical method to solve non-linear ordinary and partial differential equations [19, 20]. The key feature of the HAM lies in introducing an auxiliary parameter in the Homotopy function to accelerate the solution's convergence. Given its complexity, we chose the HAM to determine the

radial and axial components of the velocity vector in both the models developed in this work.

To begin with, in this HAM, the velocity components $u(r,z,t)$ and $w(r,z,t)$ are written in the form of series expansions in terms of an embedding parameter p ($0 \leq p \leq 1$) as follows:

$$u(r,z,t) = u_0(r,z,t) + u_1(r,z,t) * p + u_2(r,z,t) * p^2 + u_3(r,z,t) * p^3 + \cdots \quad (22)$$
and
$$w(r,z,t) = w_0(r,z,t) + w_1(r,z,t) * p + w_2(r,z,t) * p^2 + w_3(r,z,t) * p^3 + \cdots \quad (23)$$

This step is followed by defining homotopy functions for each of the governing equations. For the Newtonian fluid model, the homotopy functions for the continuity equation and the momentum equation in z-direction are shown in expressions (24) and (25) respectively:

$$H_1^N(p) = (1-p)\left(\frac{\partial^2 u}{\partial r^2}\right) + h*p*\left(\frac{\partial u}{\partial r} + \frac{1}{r}u + \frac{\partial w}{\partial z}\right) \quad (24)$$

and

$$H_2^N(p) = (1-p)\left(\frac{\partial^2 w}{\partial r^2}\right) + k*p*\left(\frac{\partial w}{\partial t} + u\frac{\partial w}{\partial r} + w\frac{\partial w}{\partial z} + P^* - \frac{1}{\alpha^2}\left(\frac{\partial^2 w}{\partial r^2} + \frac{1}{r}\frac{\partial w}{\partial r} + \Delta^2\frac{\partial^2 w}{\partial z^2}\right)\right) \quad (25)$$

For the Couple Stress fluid model, they are defined as:

$$H_1^C(p) = (1-p)\left(\frac{\partial u}{\partial r} - \frac{\partial u_0}{\partial r}\right) + l*p\left(\frac{\partial u}{\partial r} + \frac{u}{r} + \frac{\partial w}{\partial z}\right) \quad (26)$$

$$H_2^C(p) = (1-p)\left(\frac{\partial^4 w}{\partial r^4} - \frac{\partial^4 w_0}{\partial r^4}\right) + n*p\left(\frac{\partial w}{\partial t} + u\frac{\partial w}{\partial r} + w\frac{\partial w}{\partial z} + P^* + \frac{1}{\alpha^2}\left(\frac{\partial^2 w}{\partial r^2} + \frac{1}{r}\frac{\partial w}{\partial r}\right) + C\left(\frac{\partial^4 w}{\partial r^4} - \frac{2}{r}\frac{\partial^3 w}{\partial r^3} - \frac{1}{r^2}\frac{\partial^2 w}{\partial r^2} + \frac{1}{r^3}\frac{\partial w}{\partial r} + \Delta^2\left(\frac{1}{r}\frac{\partial^3 w}{\partial r\partial z^2} + \frac{\partial^4 w}{\partial r^2\partial z^2} + \Delta^2\frac{\partial^4 w}{\partial z^4}\right)\right)\right) \quad (27)$$

where h, k, l and n are the auxiliary parameters.

Since the variables $u(r,z,t)$ and $w(r,z,t)$ are expressed in series expansion form as in (22), (23), the homotopy functions also transform to series. Assuming $u_0(r,z,t)$ and $w_0(r,z,t)$ to be zero, the coefficients of each exponent of p, starting from p^1, in the R.H.S of (24), (25), (26) and (27), which are systems of PDEs in u_i and w_i are collected and equated to zero. These PDE systems are subsequently solved along with appropriate boundary conditions, as shown below in Sections 3.1 (Newtonian fluid model) and 3.2 (Couple Stress fluid model).
Known the velocity components, we derived the expression for WSS (Wall Shear Stress) for the

Newtonian model using the constitutive equation given in [6] and for the couple stress model using [14]. We also obtained the volumetric flux (QF) for both models. These expressions evaluated for various model parameters (termed as independent variables) form the inputs (termed as dependant variables) to the statistical models presented in Section 5.

3.1 Newtonian Fluid Model

The first iteration involves solving the PDEs formed by collecting the coefficients of p^1 from the R.H.S of (24) and (25) and equating them to zero. The PDEs, along with the boundary conditions, are given by:

$$\frac{\partial^2 u_1}{\partial r^2} = 0, \tag{28}$$

$$k \frac{a_0 + a_1 \cos t}{\rho \Omega^2 L^2} + \frac{\partial^2 w_1}{\partial r^2} = 0 \tag{29}$$

and

$$u_1 = \frac{\partial R}{\partial t}, w_1 = 0 \text{ on } r = R(z, t)$$

$$u_1 = 0, \frac{\partial w_1}{\partial r} = 0 \text{ at } r = 0 \tag{30}$$

The above PDEs, along with the boundary conditions, are solved for u_1 and w_1 using MATHEMATICA software. Similarly, the expressions for u_2 and w_2 are obtained by collecting the coefficients of p^2 from the homotopy functions. The PDEs and boundary conditions leading to u_2 and w_2 are given by:

$$-\frac{h\beta}{1-\beta t} - hkf(1-fz)(1-\beta t)\frac{a_0 + a_1 \cos t}{\rho \Omega^2 L^2} + \frac{\partial^2 u_2}{\partial r^2} = 0, \tag{31}$$

$$\left(k + \frac{k^2}{\alpha} + \frac{k^2}{r\alpha} - \frac{\Delta^2 k^2 f^2 (1-\beta t)}{\alpha} - \frac{k^2 \beta (1-fz)^2}{2}\right) \frac{a_0 + a_1 \cos t}{\rho \Omega^2 L^2} + \left(k^2 r^2 - k^2 (1-fz)^2 (1-\beta t)\right) \frac{a_1 \sin t}{2 \rho \Omega^2 L^2} + \frac{\partial^2 w_2}{\partial r^2} = 0 \tag{32}$$

and

$$u_2 = 0, w_2 = 0 \text{ on } r = R(z, t)$$

$$u_2 = 0, \frac{\partial w_2}{\partial r} = 0 \text{ at } r = 0 \tag{33}$$

In the same way, the subsequent approximations of u_i, w_i for $i = 3, 4, 5, ...$ are obtained by solving the PDEs obtained from the coefficients of $p^3, p^4, p^5, ...$ along with the boundary conditions similar to (33). We have calculated the expressions of u_i and w_i for $i = 1$ to 5 and thus,

$$u(r, z, t) = \sum_{i=1}^{5} u_i(r, z, t),$$

$$w(r, z, t) = \sum_{i=1}^{5} w_i(r, z, t) \tag{34}$$

which are functions of r, z and t consisting of the auxiliary parameters h and k whose values are determined as described by Liao [19, 20].

For this, we fixed the values as, $z = 0.5$, $t = 1$, $f = 0.01$, $\beta = 0.1$, $\delta = 0.001$, $HR = 72$ bpm, $a_0 = 12352.46$ $Pa.m^{-1}$ and $a_1 = 5465.3$ $Pa.m^{-1}$, Now, u and w become functions of r alone consisting of the auxiliary parameters h and k. Since it is impossible to determine both the parameters at a time, using the trial and hit method, we fixed the value of h as -0.00007. Now, using 'h-curves' which are traced by plotting $\left.\frac{d^2 u}{dr^2}\right|_{r=0}$ and $\left.\frac{d^2 w}{dr^2}\right|_{r=0}$ against k, the point on x-axis where the h-curves are almost flat is noted, and that value is assigned to k. From Fig 2, we see that the value of k is -0.06. Fig 3. shows the plots of the first five approximations of $u(r, z, t)$ and $w(r, z, t)$ clearly depicting the convergence of solutions.
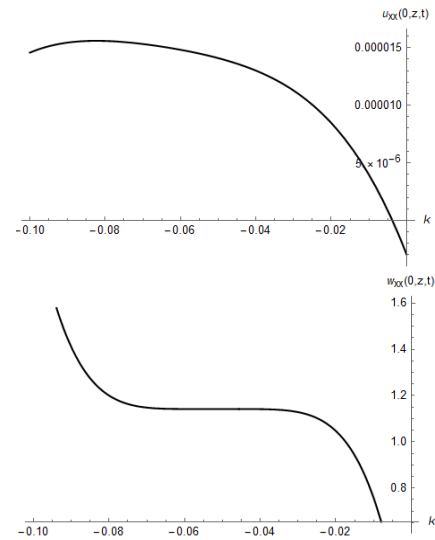

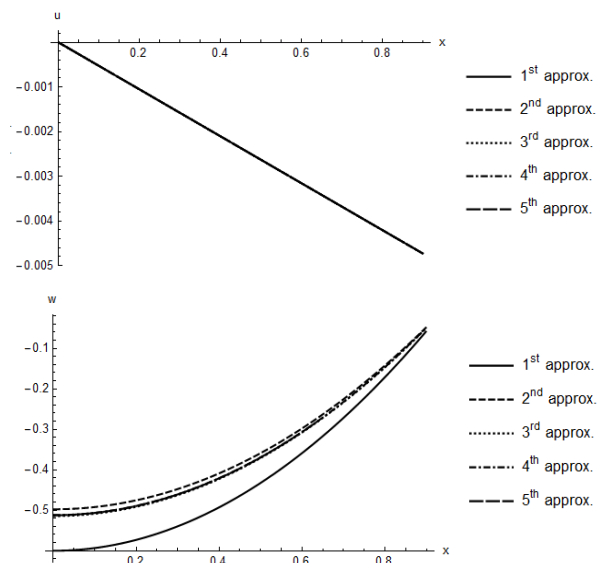**Fig. 2.** h-curves to identify the range for the auxiliary parameter 'k.'

Fig. 3. Graphs depicting the convergence of $u(r, z, t)$ and $w(r, z, t)$

A similar exercise is carried out to identify the values of parameters h and k for the other sets of model parameters.

3.2 Couple Stress Fluid Model

From expressions (26) and (27), PDEs and the respective boundary conditions for finding the first approximation is as below:

$$\frac{\partial u_1}{\partial r} = -\left(\frac{\partial w_0}{\partial z} + \frac{u_0}{r}\right), \tag{35}$$

$$\frac{\partial^4 w_1}{\partial r^4} = -n\left(\frac{\partial w_0}{\partial t} + u_0 \frac{\partial w_0}{\partial r} + w_0 \frac{\partial w_0}{\partial z} + P^* + \right.$$

$$\frac{1}{\alpha^2}\left(\frac{\partial^2 w_0}{\partial r^2} + \frac{1}{r}\frac{\partial w_0}{\partial r}\right) + C\left(\frac{\partial^4 w_0}{\partial r^4} - \frac{2}{r}\frac{\partial^3 w_0}{\partial r^3} - \frac{1}{r^2}\frac{\partial^2 w_0}{\partial r^2} + \right.$$

$$\left.\left.\frac{1}{r^3}\frac{\partial w_0}{\partial r} + \Delta^2\left(\frac{1}{r}\frac{\partial^3 w_0}{\partial r\partial z^2} + \frac{\partial^4 w_0}{\partial r^2\partial z^2} + \Delta^2\frac{\partial^4 w_0}{\partial z^4}\right)\right)\right) \tag{36}$$

And the conditions are

$$u_1 = \frac{\partial R}{\partial t}, w_1 = 0, \frac{\partial^2 w_1}{\partial r^2} - \frac{\sigma}{r}\frac{\partial w_1}{\partial r} = 0 \text{ on } r = R(z,t),$$
$$\frac{\partial^2 w_1}{\partial r^2} - \frac{\sigma}{r}\frac{\partial w_1}{\partial r} \text{ is finite at } r = 0 \text{ and } \frac{\partial w_1}{\partial r} = 0 \text{ at } r = 0. \tag{37}$$

The second approximation is then calculated in the same way using the boundary conditions:

$$u_2 = 0, w_2 = 0 \text{ on } r = R(z,t),$$
$$\frac{\partial^2 w_2}{\partial r^2} - \frac{\sigma}{r}\frac{\partial w_2}{\partial r} = 0 \text{ on } r = R(z,t),$$
$$\frac{\partial^2 w_2}{\partial r^2} - \frac{\sigma}{r}\frac{\partial w_2}{\partial r} \text{ is finite at } r = 0 \text{ and}$$
$$\frac{\partial w_2}{\partial r} = 0 \text{ at } r = 0 \tag{38}$$

We obtained convergence in the third approximation for l, n identified as -0.0007 and -0.0003, respectively (calculated by following the similar procedure described for the Newtonian model). The plots presented in Fig. 4 show the convergence of the velocity components.
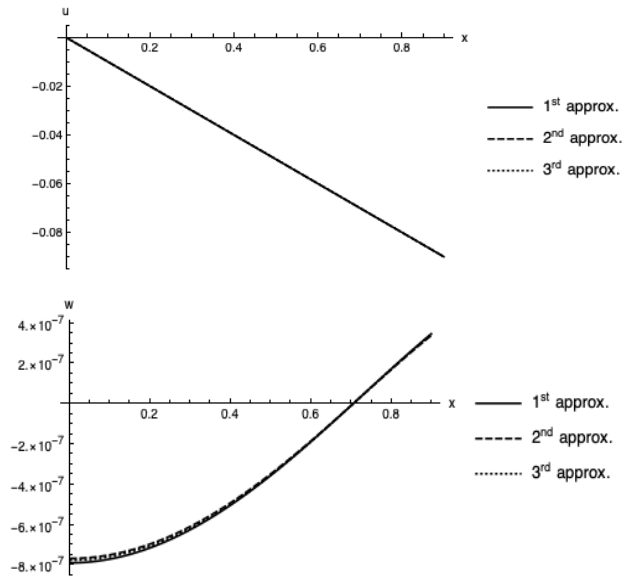
Fig. 4. Convergence plots of $u(r,z,t)$ and $w(r,z,t)$

3.3 Validation

We compared our findings with the benchmark problems to verify our work, and the particulars are as in Table 1. We compared the axial velocity component computed at various points along the radial line for the first age group using the next section's data in Tables 2 to 5. By considering the values of various parameters as, $R_0 = 0.0041\,m$, $a_0 = 12352.4\,Pa$, $a_1 = 0$, $HR = 72$ beats per minute, $\rho = 1058.1\,kg.m^{-3}$, $\mu = 0.00619\,Pa.s$ in the Poiseuille flow model and our model (with F and β zero), the axial velocity is computed and is presented in Table 1.

Table 1. Comparison of the axial velocity component

r	Present (Model-1)	Poiseuille Model
R_0	-1.0842(-19)	0
$R_0/2$	-0.0628973	-0.0628973
$R_0/4$	-0.0786216	-0.0786216
0	-0.0838631	-0.0838631

The findings are well in line with the values measured using the models used for validation.

4 Data

Table 2(a) presents the Newtonian model and the Couple Stress fluid model's parameter values based on the respective mathematical requirements (presented in Section 2).

Table 2(a). Values of the material parameters of the pipe (artery).

f	β	Δ	
		Newtonian Model	**Couple Stress Model**
0.01(f_1) 0.03 (f_2) 0.05 (f_3) 0.07 (f_4) 0.09 (f_5) 0.1 (f_6)	-0.05 (β_1) -0.01 (β_2) 0 (β_3) 0.01 (β_4) 0.05 (β_5)	0.001 0.00001	0.01 0.001 0.0001 0.00001

Table 2(b) provides a healthy individual's blood density and viscosity values from clinical data [22-25]. Further, these tables also show mathematical notations for each of the model parameters' values used in this paper's later sections. For instance, f_1 denotes the value of 0.01 of the taper fraction, similarly β_1 stands for the value of -0.05 of the expanding/contracting parameter and so on. Table 2(c) shows values assigned to the couple stress fluid parameter.

Table 2(b). Values of fluid parameters

ρ	μ
1055 (ρ_1)	1055 (ρ_1)
1058.1 (ρ_2)	1058.1 (ρ_2)
1061.2 (ρ_3)	1061.2 (ρ_3)

Table 2(c). Values assumed for fluid parameters in Couple Stress Fluid Model in addition to those in Table 1(b).

σ
0.1(σ_1)
0.3(σ_2)
0.5(σ_3)
0.7(σ_4)
0.9(σ_5)

Based on the values of Δ, shown in Table 2(a), we categorised the arteries as small and large arteries, wherein $\Delta = 0.001$ in the Newtonian model and $\Delta = 0.01$ in the Couple stress fluid model describe large artery, and $\Delta = 0.00001$ in both the models, a small artery.

While the parameters presented in Tables 2(a)-2(c) are uniform for all age groups and genders, parameters such as the heart rate values and blood pressure are age and gender-specific and presented in Table 3. This table provides data from the literature on the heart rate and the average blood pressure for each age group for male and female populations. Furthermore, the third and fifth columns show the heart rate values taken to carry out the simulations.

5 Statistical test

This section presents the details of the statistical tests performed and the analyses. Wall shear stress (WSS) and volumetric flow rate (QF) are assumed to be dependent on taper fraction (f), expanding/contracting parameter (β), couple stress parameter (σ), density (ρ), viscosity (μ), heart rate (HR) and blood pressure (BP). Most importantly, this study defines all these independent variables as categorical, and tests are carried out to identify their significant values.

5.1 Preliminary Analysis

We performed a normality test on the data generated using the Newtonian model to identify the two dependent variables, i.e., WSS and QF behaviour. Since the independent variables are assumed categorical, we used Kolmogorov – Smirnov normality test in the SPSS package at a 0.1 level of significance. The test details in the case of large arteries are presented in Table 4. The Q-Q plots depict these two variables' deviation from normality in Fig. 2 and 3.

Test for normality of the two continuous variables WSS and QF in the Couple Stress fluid model's data is also performed. Results demonstrate that the two dependent variables are also not normal variates.

Table 3. Values of heart rate and blood pressure in Newtonian and Couple stress fluid models.

Age Group	Heart Rate (HR)				Blood Pressure[26]	
	Female		Male		Female	Male
	Data from the literature [25]	Values considered	Data from the literature [25]	Values considered		
19-24 (g_1)	70-73	70 (c_1),72 (c_2),73 (c_3)	70-73	70(d_1),72(d_3),73(d_4)	120/79	120/79
25-29 (g_2)	73-76	73 (c_3),75 (c_5),76 (c_6)	71-74	71(d_2),73(d_4),74(d_5)	120/80	121/80
30-35 (g_3)	73-76	73 (c_3),75 (c_5),76 (c_6)	71-74	71(d_2),73(d_4),74(d_5)	122/81	123/82
36-39 (g_4)	74-78	74 (c_4),76 (c_6),78 (c_8)	71-75	71(d_2),73(d_4),75(d_6)	123/82	124/83
40-45 (g_5)	74-78	74 (c_4),76 (c_6),78 (c_8)	71-75	71(d_2),73(d_4),75(d_6)	124/83	125/83
46-49 (g_6)	74-77	74 (c_4),76 (c_6),77 (c_7)	72-76	72(d_3),74(d_5),76(d_7)	126/84	127/84
50-55 (g_7)	74-77	74 (c_4),76 (c_6),77 (c_7)	72-76	72(d_3),74(d_5),76(d_7)	129/85	128/85
56-59 (g_8)	74-77	74 (c_4),76 (c_6),77 (c_7)	72-75	72(d_3),74(d_5),75(d_6)	130/86	131/87
≥60 (g_9)	73-76	73 (c_3),75 (c_5),76 (c_6)	70-73	70(d_1),72(d_3),73(d_4)	134/84	135/88

Table 4. Tests of Normality for all age groups– Newtonian and Couple Stress Fluid Models.

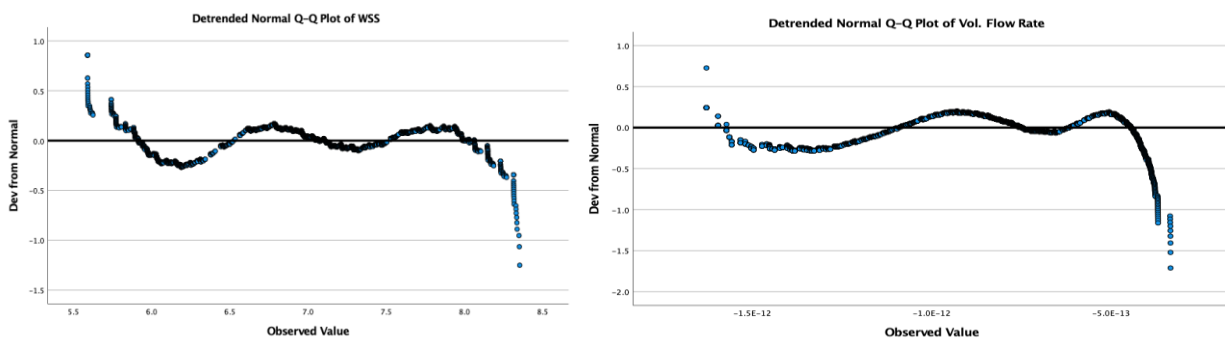|	Kolmogorov-Smirnov[a]					
	Statistic		df		Sig.	
	Newtonian Model	Couple Stress Fluid Model	Newtonian Model	Couple Stress Fluid Model	Newtonian Model	Couple Stress Fluid Model
WSS	0.067	.238	7290	36450	<.001	<.001
QF	0.076	.229	7290	36450	<.001	<.001

a. Lilliefors Significance Correction

Fig. 5: Plots showing the deviation of WSS and QF from Normality in the Newtonian Fluid Model
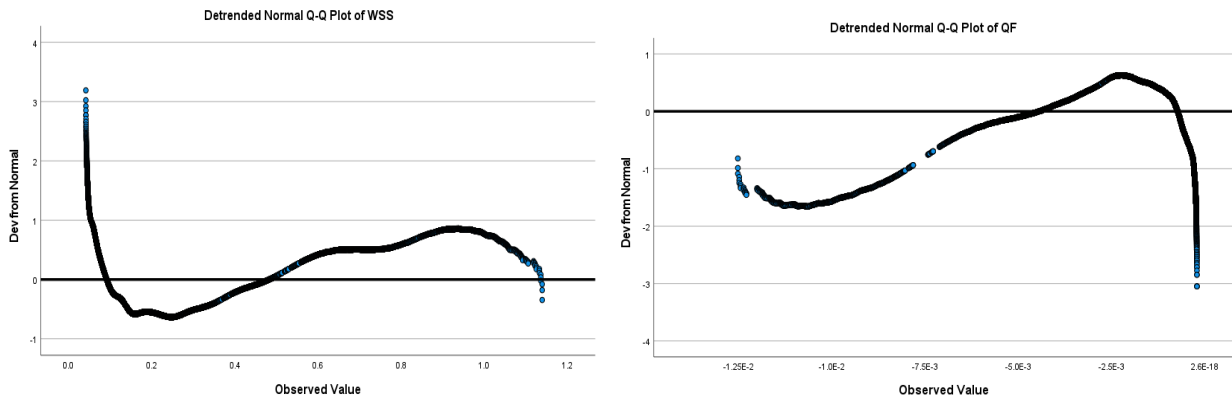
Fig. 6: Plots showing the deviation of WSS and QF from Normality in Couple Stress Fluid Model.

5.2 Primary analyses

This section presents the descriptive statistics of the variables used in the analyses in section 5.2.1, the statistical tests used, and the conclusions drawn based on the test's outputs in the subsequent sections.

5.2.1   Descriptive statistics

Tables 5 to 8 provide the descriptive statistics for each age group in the female population for the Newtonian and the Couple Stress models.

Table 5. Agewise Descriptive Statistics for Newtonian Fluid Large Artery Model for Female Population.

		g_1				g_2				g_3	
	N	Mean	Std. Deviation		N	Mean	Std. Deviation		N	Mean	Std. Deviation
HR	810	71.67	1.25	HR	810	74.67	1.25	HR	810	74.67	1.25
a_0	810	12352.50	.00	a_0	810	12441.30	.00	a_0	810	12619.10	.00
a_1	810	5465.30	.00	a_1	810	5332.00	.00	a_1	810	5465.30	.00
WSS	810	6.75	.56	WSS	810	6.76	.56	WSS	810	6.86	.57
QF	810	-8.16E-13	2.73E-13	QF	810	-8.17E-13	2.74E-13	QF	810	-8.27E-13	2.77E-13
		g_4				g_5				g_6	
	N	Mean	Std. Deviation		N	Mean	Std. Deviation		N	Mean	Std. Deviation
HR	810	76.00	1.63	HR	810	76.00	1.63	HR	810	75.67	1.25
a_0	810	12752.40	.00	a_0	810	12885.70	.00	a_0	810	13063.40	.00
a_1	810	5465.30	.00	a_1	810	5465.30	.00	a_1	810	5598.60	.00
WSS	810	6.93	.58	WSS	810	6.99	.58	WSS	810	7.10	.59
QF	810	-8.38E-13	2.81E-13	QF	810	-8.45E-13	2.84E-13	QF	810	-8.58E-13	2.88E-13
		g_7				g_8				g_9	
	N	Mean	Std. Deviation		N	Mean	Std. Deviation		N	Mean	Std. Deviation
HR	810	75.67	1.25	HR	810	75.67	1.25	HR	810	74.67	1.25
a_0	810	13285.60	.00	a_0	810	13418.90	.00	a_0	810	13418.90	.00
a_1	810	5865.20	.00	a_1	810	5865.20	.00	a_1	810	6665.00	.00
WSS	810	6.75	.56	WSS	810	7.30	.61	WSS	810	7.42	.62
QF	810	-8.16E-13	2.73E-13	QF	810	-8.83E-13	2.97E-13	QF	810	-8.97E-13	3.01E-13

Table 6. Agewise Descriptive Statistics for Newtonian Fluid Small Artery Model for Female Population.

		g_1				g_2				g_3	
	N	Mean	Std. Deviation		N	Mean	Std. Deviation		N	Mean	Std. Deviation
HR	810	71.67	1.25	HR	810	74.67	1.25	HR	810	74.67	1.25
a_0	810	12352.50	.00	a_0	810	12441.30	.00	a_0	810	12619.10	.00
a_1	810	5465.30	.00	a_1	810	5332.00	.00	a_1	810	5465.30	.00
WSS	810	2.20E19	9.74E18	WSS	810	1.80E19	7.95E18	WSS	810	1.74E19	7.78E18

| QF | 810 | -2.56 | 1.27 | QF | 810 | -2.09 | 1.03 | QF | 810 | -2.03 | 1.01 |

	g_4				g_5				g_6		
	N	Mean	Std. Deviation		N	Mean	Std. Deviation		N	Mean	Std. Deviation
HR	810	76.00	1.63	HR	810	76.00	1.63	HR	810	75.67	1.25
a_0	810	12752.40	.00	a_0	810	12885.70	.00	a_0	810	13063.40	.00
a_1	810	5465.30	.00	a_1	810	5465.30	.00	a_1	810	5598.60	.00
WSS	810	1.69E19	7.57E18	WSS	810	1.71E19	7.65E18	WSS	810	1.77E19	7.80E18
QF	810	-1.97	.98	QF	810	-1.99	.99	QF	810	-2.06	1.01

	g_7				g_8				g_9		
	N	Mean	Std. Deviation		N	Mean	Std. Deviation		N	Mean	Std. Deviation
HR	810	75.67	1.25	HR	810	75.67	1.25	HR	810	74.67	1.25
a_0	810	13285.60	.00	a_0	810	13418.90	.00	a_0	810	13418.90	.00
a_1	810	5865.20	.00	a_1	810	5865.20	.00	a_1	810	6665.00	.00
WSS	810	1.80E19	7.97E18	WSS	810	1.82E19	8.03E18	WSS	810	1.97E19	8.72E18
QF	810	-2.10	1.03	QF	810	-2.12	1.04	QF	810	-2.30	1.13

Table 7. Agewise Descriptive Statistics for Couple Stress Fluid Large Artery Model for Female Population.

	g_1				g_2					g_3	
	N	Mean	Std. Deviation		N	Mean	Std. Deviation		N	Mean	Std. Deviation
HR	4050	71.67	1.25	HR	4050	74.67	1.25	HR	4050	74.67	1.25
a_0	4050	12352.50	.00	a_0	4050	12441.30	.00	a_0	4050	12619.10	.00
a_1	4050	5465.30	.00	a_1	4050	5332.00	.00	a_1	4050	5465.30	.00
WSS	4050	.26	.25	WSS	4050	.24	.23	WSS	4050	.24	.24
QF	4050	-2.08E-3	2.27E-3	QF	4050	-1.93E-3	2.10E-3	QF	4050	-1.96E-3	2.13E-3

	g_4				g_5				g_6		
	N	Mean	Std. Deviation		N	Mean	Std. Deviation		N	Mean	Std. Deviation
HR	4050	76.00	1.63	HR	4050	76.00	1.63	HR	4050	75.67	1.25
a_0	4050	12752.40	.00	a_0	4050	12885.70	.00	a_0	4050	13063.40	.00
a_1	4050	5465.30	.00	a_1	4050	5465.30	.00	a_1	4050	5598.60	.00
WSS	4050	.24	.23	WSS	4050	.24	.23	WSS	4050	.24	.24
QF	4050	-1.91E-3	2.08E-3	QF	4050	-1.92E-3	2.10E-3	QF	4050	-1.97E-3	2.14E-3

	g_7				g_8				g_9		
	N	Mean	Std. Deviation		N	Mean	Std. Deviation		N	Mean	Std. Deviation
HR	4050	75.67	1.25	HR	4050	75.67	1.25	HR	4050	74.67	1.25
a_0	4050	13285.60	.00	a_0	4050	13418.90	.00	a_0	4050	13418.90	.00
a_1	4050	5865.20	.00	a_1	4050	5865.20	.00	a_1	4050	6665.00	.00
WSS	4050	.25	.24	WSS	4050	.25	.25	WSS	4050	.26	.26
QF	4050	-2.01E-3	2.19E-3	QF	4050	-2.03E-3	2.21E-3	QF	4050	-2.11E-3	2.30E-3

Table 8. Agewise Descriptive Statistics for Couple Stress Fluid Small Artery Model for Female Population

	g_1				g_2					g_3	
	N	Mean	Std. Deviation		N	Mean	Std. Deviation		N	Mean	Std. Deviation
HR	4050	71.67	1.25	HR	4050	74.67	1.25	HR	4050	74.67	1.25
a_0	4050	12352.50	.00	a_0	4050	12441.30	.00	a_0	4050	12619.10	.00
a_1	4050	5465.30	.00	a_1	4050	5332.00	.00	a_1	4050	5465.30	.00
WSS	4050	1.82E+6	3.98E+6	WSS	4050	1.55E+6	3.39E+6	WSS	4050	1.58E+6	3.44E+6
QF	4050	-14.51	36.20	QF	4050	-12.35	30.80	QF	4050	-12.54	31.28

	g_4				g_5				g_6		
	N	Mean	Std. Deviation		N	Mean	Std. Deviation		N	Mean	Std. Deviation
HR	4050	76.00	1.63	HR	4050	76.00	1.63	HR	4050	75.67	1.25
a_0	4050	12752.40	.00	a_0	4050	12885.70	.00	a_0	4050	13063.40	.00
a_1	4050	5465.30	.00	a_1	4050	5465.30	.00	a_1	4050	5598.60	.00
WSS	4050	1.48E+6	3.25E+6	WSS	4050	1.50E+6	3.28E+6	WSS	4050	1.54E+6	3.37E+6

	N	Mean	Std. Deviation		N	Mean	Std. Deviation		N	Mean	Std. Deviation
QF	4050	-11.81	29.51	QF	4050	-11.92	29.78	QF	4050	-12.29	30.66
g_7				g_8				g_9			
HR	4050	75.67	1.25	HR	4050	75.67	1.25	HR	4050	74.67	1.25
a_0	4050	13285.60	.00	a_0	4050	13418.90	.00	a_0	4050	13418.90	.00
a_1	4050	5865.20	.00	a_1	4050	5865.20	.00	a_1	4050	6665.00	.00
WSS	4050	1.58E+6	3.44E+6	WSS	4050	1.59E+6	3.47E+6	WSS	4050	1.70E+6	3.72E+6
QF	4050	-12.54	31.28	QF	4050	-12.65	31.56	QF	4050	-13.55	33.80

5.2.2 Primary Objectives

In this section, we present the objectives taken for the study. As our primary aim is to identify in-significant values of each model parameter; hence, we formulated the following eight objectives:

(1) To study if there is a significant difference in WSS with f in a given age group.
(2) To study if there is a significant difference in WSS with β in a given age group.
(3) To study if there is a significant difference in WSS with σ in a given age group.
(4) To study if there is a significant difference in WSS with μ in a given age group.
(5) To study if there is a significant difference in WSS with ρ in a given age group.
(6) To study if there is a significant difference in WSS with HR in a given age group.
(7) To study if there is a significant difference in QF with the above set of parameters in a given age group.
(8) To study the pairwise significance of the values of each of the independent variables in a given age group.

These objectives are all tested among each age group for the two mathematical models in male and female populations. Sample analysis for the objective (1) test is shown in section 5.2.3.

5.2.3 Analysing objective (1)

Since our preliminary study indicated that WSS is a non-normal variate, we performed the Kruskal-Wallis 1–way ANOVA test to study the significant difference in WSS with f in each age group. Tables 9 and 10 present the test's details for the female population's first age group in the Newtonian model.

5.2.3a Conclusion on Objective (1)

Table 9 shows that there is a significant difference in WSS values computed for different taper fraction values for blood flow in large arteries.

However, there is no significant difference in WSS with f in the small arteries, as seen in Table 10. Thus, we conclude that all six values assigned to f (see

Table 2(a)) mimic the same status of the arterial system in the case of small arteries.

Table 9. Newtonian Female Large Artery for g_1 – WSS

Null Hypothesis	Sig.[a,b]	Test Statistic[c]	Degrees of Freedom	Decision
The distribution of WSS is the same across categories of Taper Fraction	<0.001	68.746	5	Reject the null hypothesis

a. The significance level is 0.1.
b. Asymptotic significance (2-sided) is displayed.
c. The test statistic is adjusted for the ties.

Table 10. Newtonian Female Small Artery for g_1 – WSS

Null Hypothesis	Sig.[a,b]	Test Statistic[c]	Degrees of Freedom	Decision
The distribution of WSS is the same across categories of Taper Fraction	.860	1.922	5	Retain the null hypothesis

a. The significance level is 0.1.
b. Asymptotic significance (2-sided) is displayed.
c. The test statistic is adjusted for the ties.

Further to the analysis presented in Table 9, we identify where the difference occurs by performing the Dunn-Bonferroni post hoc test, and the results are shown in Table 11.

Table 11. Pairwise Comparison for Newtonian Model Large Artery for g_1 – WSS

Sample 1-Sample 2[a]	Test Statistic	Std. Test Statistic	Sig.[b]	Adjusted Sig.[b,c]
$f_6 - f_5$	25.233	.886	.376	1.000
$f_6 - f_4$	68.122	2.392	.017	.251
$f_6 - f_3$	112.874	3.964	<0.001	<0.001
$f_6 - f_2$	154.359	5.420	<0.001	<0.001
$f_6 - f_1$	192.300	6.753	<0.001	<0.001
$f_5 - f_4$	42.889	1.506	.132	1.000
$f_5 - f_3$	87.641	3.077	.002	.031
$f_5 - f_2$	129.126	4.534	<0.001	<0.001

$f_5 - f_1$	167.067	5.867	<0.001	<0.001
$f_4 - f_3$	44.752	1.571	.116	1.000
$f_4 - f_2$	86.237	3.028	.002	.037
$f_4 - f_1$	124.178	4.360	<0.001	<0.001
$f_3 - f_2$	41.485	1.457	.145	1.000
$f_3 - f_1$	79.426	2.789	.005	.079
$f_2 - f_1$	37.941	1.332	.183	1.000

a. Each row tests the null hypothesis that Sample 1 and Sample 2 distributions are the same.
b. Asymptotic significances (2-sided tests) are displayed. The significance level is 0.1.
c. Significance values have been adjusted by the Bonferroni correction for multiple tests.

This table indicates the significant values of f on WSS for the group g_1 as f_1, f_3 and f_5.

5.2.3a Conclusion on Objective 1 (contd.)

We carried out an analysis similar to this to test the objective (1) on data generated using the Couple Stress model and presented the details in Tables 12 and 13. We see that, in this case, the taper fraction is significant on WSS in both large and small arteries.

Table 12. Couple Stress Female Large Artery for g_1 – WSS

Null Hypothesis	Sig.[a,b]	Test Statistic[c]	Degrees of Freedom	Decision
The distribution of WSS is the same across categories of Taper Fraction	<0.001	26.903	5	Reject the null hypothesis

a. The significance level is 0.1.
b. Asymptotic significance (2-sided) is displayed.
c. The test statistic is adjusted for the ties.

Table 13. Couple Stress Female Small Artery for g_1 – WSS

Null Hypothesis	Sig.[a,b]	Test Statistic[c]	Degrees of Freedom	Decision
The distribution of WSS is the same across categories of Taper Fraction	0.005	16.730	5	Reject the null hypothesis

a. The significance level is 0.1.
b. Asymptotic significance (2-sided) is displayed.
c. The test statistic is adjusted for the ties.

Further, we discussed where the difference occurs by performing a pairwise analysis on the data of g_1 using the Dunn-Bonferroni post hoc method, the results are in Tables 14 and 15.

Table 14. Pairwise Comparison for Couple Stress Large Artery for g_1 – WSS

Sample 1-Sample 2[a]	Test Statistic	Std. Test Statistic	Sig.[b]	Adjusted Sig.[b,c]
$f_6 - f_5$	30.218	.475	.635	1.000
$f_6 - f_4$	87.562	1.376	.169	1.000
$f_6 - f_3$	148.862	2.339	.019	.290
$f_6 - f_2$	212.349	3.336	.001	.013
$f_6 - f_1$	267.422	4.202	< .001	< .001
$f_5 - f_4$	57.344	.901	.368	1.000
$f_5 - f_3$	118.644	1.864	.062	.935
$f_5 - f_2$	182.131	2.862	.004	.063
$f_5 - f_1$	237.204	3.727	< .001	.003
$f_4 - f_3$	61.300	.963	.335	1.000
$f_4 - f_2$	124.787	1.961	.050	.749
$f_4 - f_1$	179.860	2.826	.005	.071
$f_3 - f_2$	63.487	.997	.319	1.000
$f_3 - f_1$	118.560	1.863	.062	.937
$f_2 - f_1$	55.073	.865	.387	1.000

a. Each row tests the null hypothesis that Sample 1 and Sample 2 distributions are the same.
b. Asymptotic significances (2-sided tests) are displayed. The significance level is 0.1.
c. Significance values have been adjusted by the Bonferroni correction for multiple tests.

Table 15. Pairwise Comparison for Couple Stress Small Artery for g_1 – WSS

Sample 1-Sample 2[a]	Test Statistic	Std. Test Statistic	Sig.[b]	Adjusted Sig.[b,c]
$f_6 - f_5$	23.776	.374	.709	1.000
$f_6 - f_4$	70.006	1.100	.271	1.000
$f_6 - f_3$	116.625	1.832	.067	1.000
$f_6 - f_2$	165.462	2.600	.009	.140
$f_6 - f_1$	212.419	3.337	.001	.013
$f_5 - f_4$	46.230	.726	.468	1.000
$f_5 - f_3$	92.849	1.459	.145	1.000
$f_5 - f_2$	141.686	2.226	.026	.390
$f_5 - f_1$	188.643	2.964	.003	.046
$f_4 - f_3$	46.619	.732	.464	1.000
$f_4 - f_2$	95.456	1.500	.134	1.000
$f_4 - f_1$	142.413	2.238	.025	.379
$f_3 - f_2$	48.837	.767	.443	1.000
$f_3 - f_1$	95.794	1.505	.132	1.000
$f_2 - f_1$	46.957	.738	.461	1.000

a. Each row tests the null hypothesis that Sample 1 and Sample 2 distributions are the same.
b. Asymptotic significances (2-sided tests) are displayed. The significance level is 0.1.
c. Significance values have been adjusted by the Bonferroni correction for multiple tests.

From Tables 14 and 15, we see that the p-value between some pairs (f_i, f_j) is more than 0.1, and thus the data sets with these values of 'f'form the redundant data set. The list of taper fraction values significant on WSS for both the models is summarised in Table 16.

Table 16. The categories of f significant on WSS for g_1.

Newtonian Fluid Model		Couple Stress Fluid Model	
Large Artery	**Small Artery**	**Large Artery**	**Small Artery**
f_1 f_3 f_5	f_3	f_1 f_3 f_5	f_1 f_6

An exercise similar to this is carried out to identify the list of significant taper fraction values on the volumetric flow rate (QF) in the group g_1 and the results are shown in Table 17. We understand that f is significant on WSS in both large and small arteries.

Table 17. The categories of f significant on QF for g_1.

Newtonian Fluid Model		Couple Stress Fluid Model	
Large Artery	**Small Artery**	**Large Artery**	**Small Artery**
f_1 f_3 f_5	f_1 f_6	f_1 f_3 f_5	f_1 f_3 f_6

We performed statistical tests for objectives stated from (2)-(8) and summarised the outcomes of each in Tables 18 to 21.

Table 18. The significant categories of β for g_1.

WSS				QF			
Newtonian Fluid Model		Couple Stress Fluid Model		Newtonian Fluid Model		Couple Stress Fluid Model	
Large Artery	Small Artery	Large Artery	Small Artery	Large Artery	Small Artery	Large Artery	Small Artery
β_1 β_2 β_3 β_4 β_5	β_1 β_3 β_5	β_1 β_2 β_3 β_4 β_5	β_1 β_2 β_3 β_4 β_5	β_1 β_2 β_3 β_4 β_5	β_1 β_2 β_4 β_5	β_1 β_2 β_3 β_4 β_5	β_1 β_2 β_3 β_4 β_5

Table 19. The significant categories of σ in Couple Stress Model.

WSS		QF	
Large Artery	Small Artery	Large Artery	Small Artery
σ_1	σ_1	σ_1	σ_1
σ_2	σ_2	σ_2	σ_2
σ_3	σ_3	σ_3	σ_3
σ_4	σ_4	σ_4	σ_4
σ_5	σ_5	σ_5	σ_5

Table 20. The significant categories of ρ for g_1.

WSS				QF			
Newtonian Fluid Model		Couple Stress Fluid Model		Newtonian Fluid Model		Couple Stress Fluid Model	
Large Artery	Small Artery	Large Artery	Small Artery	Large Artery	Small Artery	Large Artery	Small Artery
ρ_2	ρ_2	ρ_2	ρ_2	ρ_2	ρ_2	ρ_2	ρ_2

Table 21. The significant categories of μ for g_1.

WSS				QF			
Newtonian Fluid Model		Couple Stress Fluid Model		Newtonian Fluid Model		Couple Stress Fluid Model	
Large Artery	Small Artery	Large Artery	Small Artery	Large Artery	Small Artery	Large Artery	Small Artery
μ_2	μ_1 μ_2 μ_3	μ_2	μ_1 μ_2 μ_3	μ_1 μ_2 μ_3	μ_1 μ_2 μ_3	μ_2	μ_1 μ_2 μ_3

It may be noted that the analyses and conclusions presented above are on the first age group in the female population. This analysis, when carried out, for the remaining age groups in the female population and among all the male population's age groups, resulted in similar results as presented in Tables 9-21. However, the significant heart rate values (HR) vary with the age groups in the female population; the details are in Table 22.

Table 22. The significant categories of HR in each age group in female population.

Age Group	WSS				QF			
	Newtonian Fluid Model		Couple Stress Fluid Model		Newtonian Fluid Model		Couple Stress Fluid Model	
	Large Artery	Small Artery	Large Artery	Small Artery	Large Artery	Small Artery	Large Artery	Small Artery
g_1	c_2	c_1, c_2, c_3	c_1, c_3	c_1, c_3	c_2	c_1, c_2, c_3	c_1, c_3	c_1, c_3
g_2	c_5	c_3, c_5, c_6	c_3, c_6	c_3, c_6	c_5	c_3, c_5, c_6	c_3, c_6	c_3, c_6
g_3	c_5	c_3, c_5, c_6	c_3, c_6	c_3, c_6	c_5	c_3, c_5, c_6	c_3, c_6	c_3, c_6
g_4	c_6	c_4, c_6, c_8	c_4, c_8	c_4, c_8	c_6	c_4, c_6, c_8	c_4, c_8	c_4, c_8
g_5	c_6	c_4, c_6, c_8	c_4, c_8	c_4, c_8	c_6	c_4, c_6, c_8	c_4, c_8	c_4, c_8
g_6	c_6	c_4, c_6, c_7	c_4, c_7	c_4, c_7	c_6	c_4, c_6, c_7	c_4, c_7	c_4, c_7
g_7	c_6	c_4, c_6, c_7	c_4, c_7	c_4, c_7	c_6	c_4, c_6, c_7	c_4, c_7	c_4, c_7
g_8	c_6	c_4, c_6, c_7	c_4, c_7	c_4, c_7	c_6	c_4, c_6, c_7	c_4, c_7	c_4, c_7
g_9	c_5	c_3, c_5, c_6	c_3, c_6	c_3, c_6	c_5	c_3, c_5, c_6	c_3, c_6	c_3, c_6

Finally, we could identify the model parameters' significant values on WSS and QF in each age group and for both male and female populations and thereby, the input set's redundant data. The input data set is then refined, and a comparison of the dataset's size is presented in Tables 23 and 24.

6 Conclusion

Karthik Alasakani,
Radhika S.l. Tantravahi, Praveen Kumar Ptv

This paper proposed a novel technique for identifying redundancy in the input data set for the mathematical models developed for simulating the human arterial system. The input data set consisted of a finite number of values from a range of the permissible values derived from clinical observations or mathematical constraints on the model parameters. Though the values appear to differ significantly, it is presumed that some of the generated data sets mimic the same state of the system. For instance, the values of WSS in the Newtonian model, large arteries computed at the heart rates of 70, 72 and 73 bpm in the age group g_1 with all other parameters fixed, were 7.7334, 7.73308 and 7.73301, respectively. Thus, we see not much difference in the values of WSS computed for these three data values. This paper presents statistical testing methods to identify such data values as these. We proposed the non-parametric one-way and pairwise tests, and we see from Table 9-22 that the proposed methods could efficiently identify such redundant data sets. We then computed the input data set's size by removing all such redundant or insignificant values and presented the details in Tables 23 and 24. Since the data used for simulations is on healthy individuals, this radical reduction in the data set size looks no strange. We expect that the size reduction might not be this unusual for unhealthy arteries, which we wish to explore in our next work.

Table 23. The size of input data before and after refining - Newtonian Model.

	Large Artery		Small Artery	
	Before	After	Before	After
WSS	7290	135	7290	243
QF	7290	405	7290	432

Table 24. The size of input data before and after refining - Couple Stress Model.

	Large Artery		Small Artery	
	Before	After	Before	After
WSS	36450	1350	36450	2700
QF	36450	1350	36450	4050

References:

[1] J. Tu, K. Inthavong, K.K.L. Wong, *Computational Hemodynamics, Theory, Modeling and Applications*, Springer, 2015.

[2] A. Quarteroni, Modeling the Cardiovascular System- A Mathematical Adventure: Part-II, *SIAM News*, Vol.34, No.6, 2001.

[3] D.S. Shankar, U. Lee, Mathematical modelling of pulsatile flow of non-Newtonian fluid in stenosed arteries, *Communications in Non-linear Science and numerical simulation*, Vol.74, No.7, 2009, pp. 2971-2981.

[4] P.J. Blanco, M.R. Pivello, S.A. Urquiza, R.A. Feijoo, On the potentialities of 3D–1D coupled models in hemodynamics simulations, *J. Biomech.*, Vol. 42, 2009, pp. 919–930.

[5] L. Formaggia, D. Lamponi, A. Quarteroni, One-dimensional models for blood flow in arteries, *J. Eng. Mathemat.*, Vol.47, 2003, pp. 251–276.

[6] H. Ho, G. Sands, H. Schmid, K. Mithraratne, G. Mallinson, P. Hunter, A hybrid 1D and 3D approach to hemodynamics modelling for a Patient-Specific cerebral vasculature and aneurysm. In *International Conference on Medical Image Computing and Computer-Assisted Intervention, Springer*, 2009, pp. 323–330.

[7] W. Kroon, W. Huberts, M. Bosboom, F. van de Vosse, (2012). A numerical method of reduced complexity for simulating vascular hemodynamics using coupled 0D lumped and 1D wave propagation models, *Comput. Math. Methods. Med.*, Vol.2012, 2012.

[8] F. Liang, S. Takagi, R. Himeno, H. Liu, Multiscale modeling of the human cardiovascular system with applications to aortic valvular and arterial stenoses, *Med. Biol. Eng. Comput.*, Vol.47, 2009, pp. 743–755.

[9] A.C.I. Malossi, P.J. Blanco, P. Crosetto, S. Deparis, A. Quarteroni, Implicit coupling of one-dimensional and three-dimensional blood flow models with compliant vessels, *Multiscale Modeling & Simulation*, Vol.11, 2013, pp. 474–506.

[10] M.S. Olufsen, C.S. Peskin, W.Y. Kim, E.M. Pedersen, A. Nadim, J. Larsen, Numerical simulation and experimental validation of blood flow in arteries with structured-tree outflow conditions, *Ann. Biomed. Eng.*, Vol.28, 2000, pp. 1281–1299.

[11] A. Bartosik, Simulations of Frictional Losses in a Turbulent Blood Flow Using Three Rheological Models, *WSEAS Transactions on Fluid Mechanics*, Vol.15, 2020, pp. 131-139.

[12] J.N. Mazumdar, *Biofluid Mechanics*, World Scientific, 1992.

[13] V.K. Stokes, *Theories of Fluids with Microstructure*, Springer Berlin Heidelberg, 1984.

[14] O. Bautista, A. Matias, J. Arcos, P. Escandón, Electrokinetically-driven viscoelastic fluid flow in a microchannel with hydrodynamic slipwalls, *Engineering World*, Vol.2, 2020, pp. 1-9.

[15] G. Makanda, S. Shaw, Numerical analysis of the Bivariate Local Linearization Method (BLLM) for partial differential equations in Casson fluid flow, *WSEAS Transactions on Fluid Mechanics*, Vol.14, 2019, pp. 131-141.

[16] S. Uchida, H. Aoki, Unsteady flows in a semi-infinite contracting or expanding pipe, *J. Fluid Mech.*, Vol.82, No.2, 1977, pp. 371–387.

[17] A. Karthik, K. Sashank, T.S.L. Radhika, A Study on the Effect of Various Fluid, Flow and Mechanical Parameters on the Flow of Newtonian Fluid in an Expanding and Contracting Pipe, *Mathematical Modeling and Computational Tools, ICACM 2018, Springer Proceedings in Mathematics & Statistics*, Vol.320, 2020, pp. 101-114.

[18] P.K. Mandal, An unsteady analysis of non-Newtonian blood flow through tapered arteries with a stenosis, *Int. J. Non. Linear. Mech.,* Vol.40, No.1, 2005, pp. 151–164.

[19] S. Liao, *Beyond perturbation : introduction to the homotopy analysis method*, Chapman & Hall/CRC, Boca Raton, 2004.

[20] T.S.L. Radhika, T.K.V. Iyengar, T.R. Rani, *Approximate analytical methods for solving ordinary differential equations*, CRC Press, Boca Raton, 2015.

[21] A. Karthik, T.S.L. Radhika, Praveen Kumar, An Approach to Identify Significant Parameters in Blood Flow Through Human Arteries, *Science & Technology Asia*, Vol.25, No.1, 2020, pp. 95-105.

[22] R.J. Tudnowski, R.C. Rico, Specific Gravity of Blood and Plasma at 4 and 37 ºC, *Clinical Chemistry*, Vol.20, No.5, 1974, pp. 615-616.

[23] C. Carallo et al., The effect of aging on blood and plasma viscosity. An 11.6 years follow-up study, *Clin. Hemorheol. Microcirc.*, Vol.47, No.1, 2011, pp. 67-74.

[24] V. Marchione, Resting heart rate chart: Factors that influence heart rate in elderly,. *https://www.belmarrahealth.com/resting-heart-rate-chart-factors-influence-heart-rate-elderly/*, 2018.

[25] V. Marchione, Understanding blood pressure readings key to overall well-being, *https://www.belmarrahealth.com/understanding-blood-pressure-readings-is-key-to-overall-well-being/*, 2017.

Contribution of individual authors to the creation of a scientific article (ghostwriting policy)

Creative Commons Attribution License 4.0 (Attribution 4.0 International , CC BY 4.0)